HUMS2025 Data Challenge Result Summary

Team Name: VUB

Team Members: Cédric Peeters

Institutions: Vrije Universiteit Brussel

Publishable: Yes

1. Summary of Findings

Based on the front and rear sensor, there are clear indications of the crack signature progressing in the vibration data. Depending on the chosen indicator, the time of detection differs, but the earliest detection is achieved using the modulation sidebands at 4 times the carrier frequency, i.e. 22.92Hz, as the crack is likely to be most excited by the planets passing by 4 times per carrier rotation. Tracking these sideband amplitudes and using Tukey's thresholding method results in an alarm at 23-4-2024 at 11:34:28 of the raw data at 125% load (Day010_20240423_113428_125%TT.mat) for the rear sensor. The rear sensor data at 100% load presents the first alarm at 24-4-2024 at 11:33:40. The front sensor detects it on 24-4-2024 at 10:12:21 for 100% load and at 24-4-2024 17:07:19 for 125% load. While it's difficult to discern with certainty whether the trends characterize the primary or secondary crack, the difference in detection time and trend evolution between the sensors could be indicative of the primary vs secondary crack occurring at different times and locations.

2. Description of Analysis Methods

Given the housing crack occurred on a non-rotating component near the front sensor during a run-to-failure test, the following assumptions were made to ensure the results/trends represent the housing crack propagation rather than the gear degradation test which was being run:

1. A stationary housing crack is unlikely to exhibit a perfectly repetitive fault signature (unlike gear tooth cracks).
2. A stationary housing crack is expected to introduce random noise, increasing the spectral energy in specific frequency bands. Additionally, a crack signature typically introduces high-frequency noise.
3. Changes in structural rigidity may alter the casing's modal behavior, potentially shifting resonances.
4. In a planetary gearbox with a fixed ring gear, the four passing planet gears likely excite the crack with each pass, causing signal changes at four times the planet carrier frequency. These changes are expected to manifest through either deterministic energy increases at carrier frequency harmonics, or in sidebands of the gear meshing frequencies, or through increased noise modulated by four times the carrier frequency (abbreviation used from here on out: 4 x planet carrier frequency = $4xf_{carrier}$).
5. Under run-to-failure overload, a gradual gear degradation trend is expected to appear distinctively from the more sudden housing crack propagation and should not be mistaken for the crack propagation. Especially the pinion gear sensor should showcase this degradation.

First, an ad-hoc approach is presented to illustrate the reasoning behind the search for the presence of a housing crack propagation. Afterwards, an automated approach is presented to show how the same could be achieved but in a more realistic scenario, i.e. without prior knowledge of the defect being a housing crack.

Ad-hoc "manual" approach: Since the data is measured at stationary operating conditions, it is straightforward to assess the amplitude spectra as well as the modulation spectra for both the raw and H-SSA data. Firstly, both the raw and H-SSA amplitude spectra reveal an energy increase between 14 and 18 kHz. Figure 1a shows the amplitude spectra of the raw data as measured by the Front sensor at 125% load from 13 kHz to 19 kHz, and Figure 1b tracks this same spectral band in time as a trend for all 4 sensors but for the H-SSA data.

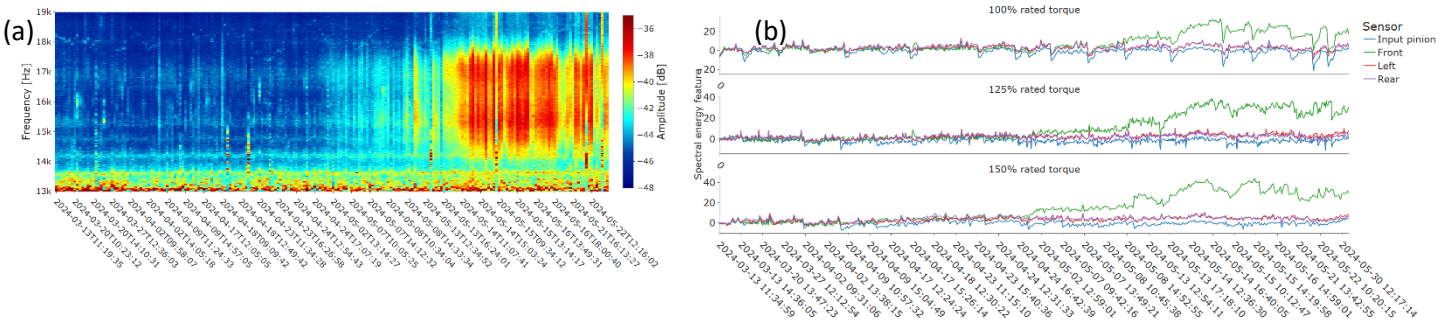

Figure 1: (left) Evolution of amplitude spectra of raw Front sensor data around 16kHz at 125% load, (right) Spectral energy in time for all 4 sensors around 16kHz in the H-SSA data[1]

Trending of the energy in this band for all the sensors and for the raw and H-SSA data reveals that only the front sensor exhibits this particular increasing trend, starting on the 2nd of May 2024. Simultaneously, no amplitude increase is observed at 22.92 Hz (= $4xf_{carrier}$) in these regular amplitude spectra. Hence, we now need to ascertain that we are actually dealing with a crack-related energy increase around 16kHz and not just a random noise increase that can potentially be due to a myriad of reasons (e.g. loosening of the sensor connection, gear wear due to the run-to-failure testing, small shifts in operating/environmental conditions, etc.). To improve our confidence, we verify if assumption nr 4 is valid for this energy increase, i.e. check whether this frequency band is modulated by $4xf_{carrier}$. We can achieve this by simply band-pass filtering from 14 kHz to 18 kHz and calculating the squared envelope spectrum of the resulting signal. The results in Figure 2 show that $4xf_{carrier}$ at 22.92 Hz (or order 0.2292 if order 1 is the 100Hz input pinion speed) becomes much more dominant at the same rate as the energy increase in the 14-22 kHz band, i.e. starting from May 2nd, thus drastically increasing the odds that this energy increase around 16 kHz is actually representative of the crack propagation.

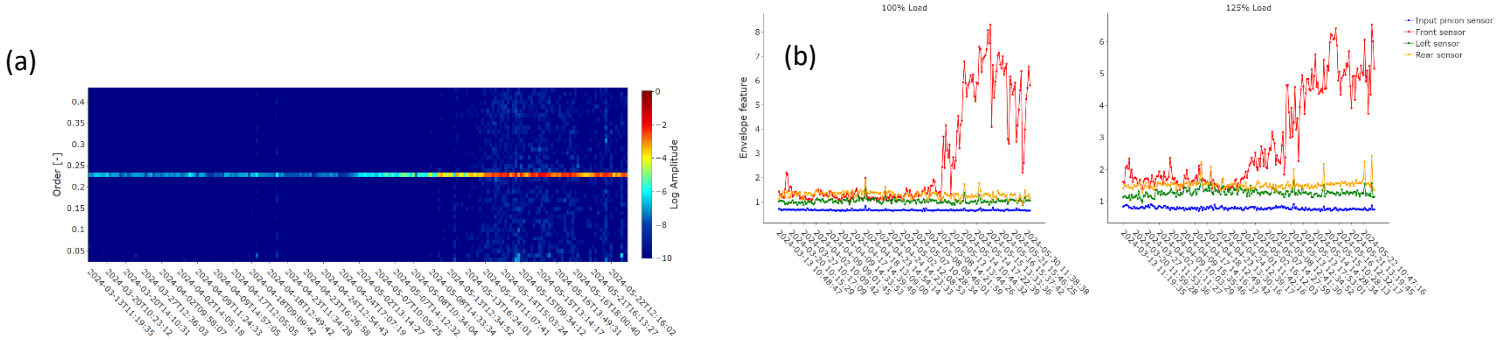

Figure 2: Squared envelope order spectra of the raw Front sensor data at 125% load, (left) Color map evolution of 4xCarrier frequency, (right) Envelope indicator trends based on the amplitude evolution of 4xcarrier frequency for 100% and 125% load for all 4 sensors.

[1] Note that the x-axis labels on all graphs are timestamps from the measurements, but that the x axis ticks themselves are non-equidistant in time to allow for the data points to be spread evenly over the graph instead of being clustered per day of testing. This improves the interpretability of the trend progression but makes reading the x-axis time evolution more complex. If this would be problematic in some way during evaluation, plots can be provided using a different x-axis.

These findings seem to corroborate the logic behind assumptions nr 1, 2, and 4, and potentially also nr 3. However, assumption nr 3 requires doing an actual operational modal analysis which was not performed as it is not of particular interest for this data challenge.

The last item to check for is any potential changes in the sideband amplitudes around the planetary gear mesh frequency. The sidebands spaced at $4xf_{carrier}$ or 22.92 Hz, can be affected by this crack as stated in assumption nr 4. Interestingly, the sidebands around the first fundamental at 568Hz barely show any evolution, while tracking the amplitude of the first 3 sidebands spaced at $4xf_{carrier}$ or 22.92Hz around the 2nd GMF harmonic at 1136Hz results in Figure 3, which shows a steady increase from the 24th of April for **both the front and rear sensor**.

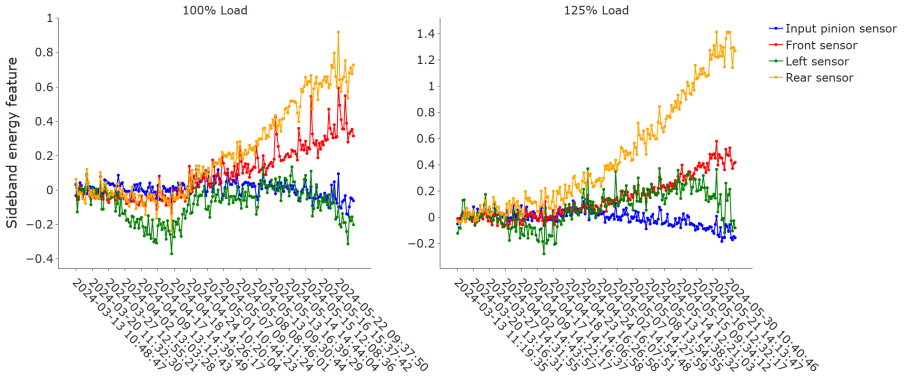

Figure 3: Energy of sideband harmonics spaced at $4xf_{carrier}$ around 2nd harmonic of 568Hz (=planetary gear mesh frequency) for the raw data of the 4 sensors (Each trend was vertically aligned around 0 for the first measurements to highlight the deviation from healthy behavior).

Automated approach: In a practical online monitoring system, the frequency band of interest at 14-18kHz would be unknown and it would be more practical to either directly target the sidebands in the autopower spectra or the harmonic at $4xf_{carrier}$ in the cyclostationary signal content as these are known frequencies and likely monitoring candidates to be indicative of degradation. The latter can be achieved using cyclic spectral correlation maps as in Ref[2], this tool allows for simultaneously tracking of both the cyclic 22.92 Hz modulation frequency and the carrier frequency band of interest, 14-18 kHz, without any prior knowledge. Due to the page limit, the reader is referred to the Ref[2] for the full details (i.e. how to track both the cyclic and carrier frequency of the fault). Lastly, assumption nr 5 was also investigated as a sanity check to verify whether there was a gradual increase noticeable in the data as would be expected from gradual gear wear. Figure 4 shows the broadband RMS level of the raw data for each sensor at 125% load. Especially the pinion gear sensor shows a slowly increasing trend in vibration energy which corresponds to the original intent of the test campaign. Inspecting the amplitude spectra (*not shown here*) for the location of this energy increase revealed that the amplitude increases are spread out over many different harmonics.

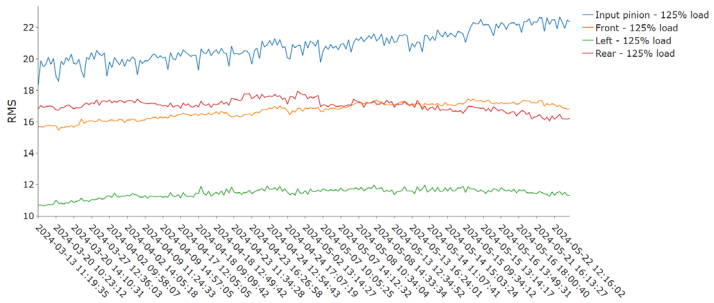

Figure 4: Gradual changes can be observed in the overall statistics of the raw vibration data.

[2] Perez-Sanjines, Fabian, Cédric Peeters, Timothy Verstraeten, Jérôme Antoni, Ann Nowé, and Jan Helsen. "Fleet-based early fault detection of wind turbine gearboxes using physics-informed deep learning based on cyclic spectral coherence." *Mechanical Systems and Signal Processing* 185 (2023): 109760.

3. Key Fault Characteristics for Early Detection

As explained in detail in the previous section and to avoid repetition, the crack progression can be detected in multiple manners:

- Via the spectral energy of the frequency band from 14 kHz to 22 kHz using front sensor, see Figure 1.
- Via the modulation signature at $4xf_{carrier}$ or 22.92 Hz using the front sensor, see Figure 2.
- Via the sidebands spaced at 22.92Hz around the planetary gear mesh frequency in the autopower spectra, specifically the 2nd GMF harmonic is the best candidate. See front and rear sensor in Figure 3.

All of these are phenomena that represent key characteristics of a housing crack progression and not of the gradual pinion gear degradation, given that the GMF fundamental harmonics show little sign of degradation nor do their sidebands spaced at their rotation frequencies.

4. Fault Progression Trending Curve

The spectral energy and modulation trends in both raw and H-SSA data are nearly identical for early detection, with alarms detected from 13:14 on May 2nd. However, the clearest fault progression and earliest detection were achieved using the sideband feature on the raw data at 125% load with rear sensor data. Figure 5 shows the alarm trends using Tukey's thresholding method, where the first 50 measurements are considered "healthy" and used to calculate the mean and interquartile range for the warning and alarm thresholds. ***The earliest red alarm value and point of detection is 23 april 2024 at 11:34:28 or measurement number 78 of the raw data at 125% load (Day010_20240423_113428_125%TT.mat) for the rear sensor***. Using the sideband feature trend of the rear and front sensors provides a quasi-linear view of the crack progression, although 2 periods of crack progression can be somewhat distinguished, i.e. zone I and II in Figure 5, where the latter showcases a faster progression than the former, starting from May 13. Additionally, Figure 6 shows the alarm trend with the same 2 periods but using the modulation features of Figure 2. Here the change from zone I to II on the 13th of May is much more noticeable as it is on that day that the modulation at 100% load for the front sensor changes completely. A strong increase can also be observed for 125% load. This can likely be attributed to the secondary crack forming. However, after the 14th of May the modulation indicator stabilizes, most likely due to the energy normalization of the indicator, and the sideband feature forms a more realistic representation of the crack progression in time.

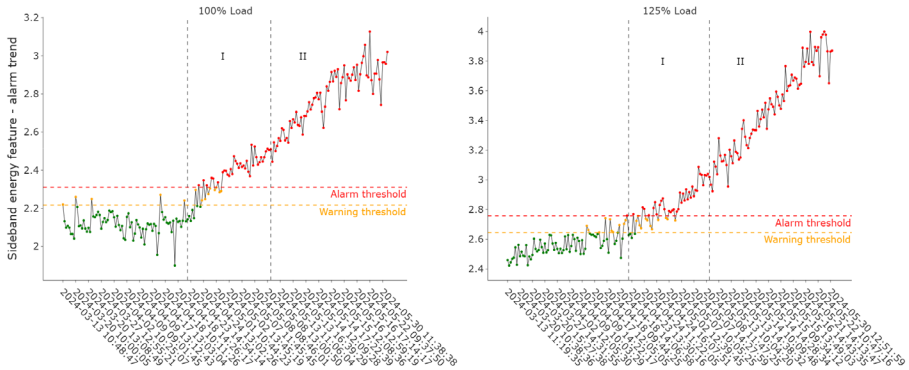

Figure 5: Alarm trends of the rear sensor sideband feature on the raw data for 100% and 125% load.

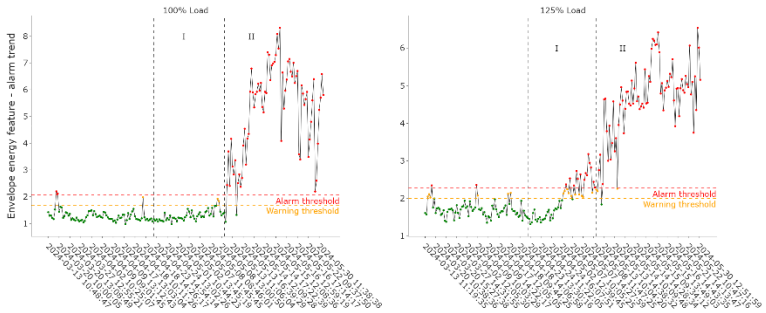

Figure 6: Alarm trend on the front sensor using Tukey's method based on the amplitude evolution of the signal modulation by 4xcarrier frequency for 100% and 125% load after filtering in the 14-18kHz band.